2nd Micro and Nano Flows Conference
West London, UK, 1-2 September 2009

# A Pressure Drop Investigation of Immiscible Liquid-Liquid Micro Flows

Oliver TAHENY[1,*], Mark DAVIES[1,2], Tara DALTON[1,2]

* Corresponding author: Tel.: +353 (0)61 202471; Email: oliver.taheny@ul.ie
1: Stokes Institute, University of Limerick, Ireland
2: Stokes Bio Ltd., Limerick, Ireland

**Abstract** Over the past decade there has been a considerable increase in the research on lab-on-a-chip applications that focuses on designing analytical chemical and biological devices. One such application is the possibility of integrating the functional steps of DNA analysis into a micro-total-analysis system (μTAS). Encapsulation of PCR samples within an inert carrier fluid allows the samples to be transported as micro-reactors. Plug based micro reactors suspended in an inert carrier fluid have a lot of promise in microfluidic analytical devices, offering a reduction in resident-time, reagents and labour with an increase in through-put, accuracy and quality. The development of a thin wetting film between the wall of the capillary and the micro reactor increase the interfacial area of the plug and can also intensify the internal circulation occurring within the plug. Only recently has work being preformed on the fluid mechanics that characterise this scale. An experimental study is carried out to study the effect capillary diameter, carrier viscosity and flow rate has on the pressure drop under bi-phasic flow conditions.

**Keywords:** Capillary micro-reactor, thin film, pressure drop, fluidic resistance, μTAS

## 1. INTRODUCTION

Work currently underway at the Stokes Institute and Stokes Bio Ltd. concerns the production of medical microfluidic diagnostic devices for the accurate early molecular diagnosis of childhood Leukaemia. All cancers have a genetic origin and are classified as heterogeneous diseases; many subtypes with many levels of expression. Advanced and precise diagnosis of the disease's sub-type can lead to a more tailored treatment for the patient. By processing the biological samples as capillary micro-reactors, a reduction in reagents and labour is achieved. Capillary micro-reactors are characterised by the flow of two immiscible liquids, with one liquid acting as the wetting carrier fluid, and the other as individual processing sub-volumes. This reduction in processing volumes offers microfluidics a huge potential for high-throughput analytical automation of biological and chemical reactions. Barrett *et al.* (2007) presents a continuous flow polymerase chain reaction (PCR) device that processes samples as discrete micro-reactors. Roper *et al.* (2005) and Sirr *et al.* (2006) also use microfluidics for DNA amplification. By transporting samples and reagents as micro-reactors in an immiscible liquid, the typical laminar flow regime takes on a form where the homogenous flow conditions are changed. These conditions include thin films, encapsulated plugs and internal circulation within individual sub-volumes. Internal circulation is an important parameter for the mixing performance of a micro-reactor. Kashid *et al.* (2005) employs computational fluid dynamics (CFD) and particle image velocimetry (PIV) to highlight the reduction in striation length with the introduction of a second immiscible liquid. This phenomenon is well documented in the literature: Burns *et al.* (2001), Sarrazin *et al.* (2006), Miessner *et al.* (2008).

Kashid *et al.* (2007) modified a bi-phasic pressure drop model developed by Charles (1963) which included the aqueous fraction. The model showed good agreement with data. Adzima *et al.* (2006) measured pressure drops for droplet flows in square micro-channels providing correlations for designing microfluidic devices. Groß *et al.* (2008) presents an empirical equation for bi-phasic pressure drop noting the influence of segment internal viscosity as an important parameter in enhanced fluidic resistance.

This work investigates the fluid dynamic characteristics of capillary micro-reactors, which are shown to create a significant rise in flow resistance. The aim is to quantify the pressure

excess attributed to an aqueous plug length and to characterise a relationship between this increase in pressure and the geometric properties that characterise the flow conditions. Data is also compared to an existing theoretical pressure drop model.

## 2. EXPERIMENTAL PROCEDURE

The experimental arrangement for the pressure drop measurements, figure 1, consisted of a Harvard Apparatus PHD 2000 precision syringe pump, set to withdrawal mode, for the actuation of the fluids. Flow direction is outlined by the arrows in the schematic. Flow rates were in the range of 3-7µl/min to match the flow rate range used by Curran *et al.* (2007), Barrett *et al.* (2007) and Sirr *et al.* (2006) for nucleic acid amplification.

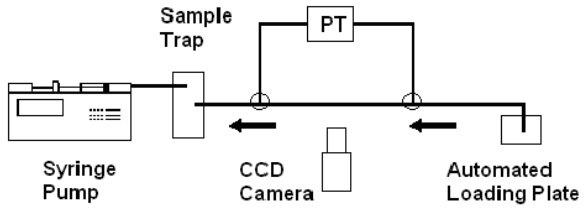


**Fig. 1** Schematic representation of experimental setup. PT represents the differential pressure transducer. Arrows indicate direction of flow. Pressure transducer is connected to capillaries via a liquid bridge (figure 2).

Ten millilitre Hamiliton Microlitre Gastight glass syringes were used, minimising the capacitance pumping evident in plastic syringes with flexible barrels. Polyetheretherketone (PEEK) fittings, availbe from Upchurch Scientific, were employed to connect the syringe to capillaries. Three different Teflon capillaries, with inner diameters of 330 µm, 400 µm and 580 µm, were characterised in immiscible liquid-liquid plug flow. Fluka silicone oil AR20 and Phenylmethylpolysiloxane PD5, with viscosities of 20 mPa.s and 4 mPa.s respectively, operated as the carrier fluids. The plugs were formed from an aqueous mix of 1% red dye, 0.1% Triton X-100 and 98.9% deionised water. The addition of the surfactant reduces the interfacial tension and permitted the passage of longer plug lengths through the liquid bridges without fouling occurring. Fouling, termed here, is the inability of an aqueous plug to pass through the liquid bridge from one capillary to another, resulting in the contamination of the liquid bridge.

The pressure transducer used was an Omega wet/wet unidirectional differential pressure transducer with an accuracy of 0.25% full scale. The transducer was pre-calibrated in compliance with ANSI/NCSL Z540-1-1994 and is certified in accordance with the National Institute of Standards and Technology.

Liquid bridges connected the pressure transducer sense lines to capillaries. This novel use of liquid

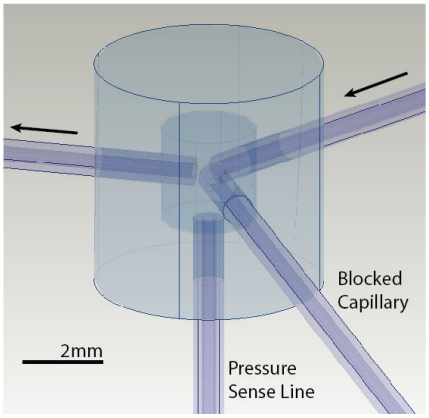


**Fig. 2** Liquid bridge geometry. Flow direction highlighted. Third in-plane capillary is unused and blocked.

bridges prevented any possibility of sense line contamination, which was found when a tee junction (Kashid *et al.*, 2007 was integrated into the system and plugs over five millimetres were investigated. A microfluidic card (Stokes Bio Ltd.) with integrated liquid bridges was adopted. Figure 2 illustrates the liquid bridge geometry, with three in plane capillaries, one of which is not used. The pressure sense line is connected out of plane line negating any interaction with the aqueous plugs. The void volume in the bridge, with no capillary tubing, is 12.27 µl. Capillaries were glued in place with a UV curable adhesive from DYMAX Europe. Epoxy, Robnor Adhesive 200 ml Twin Cartridge, encased the capillaries and liquid bridges ensuring no leaks or air contamination.

Aqueous plugs were created using an automated stage and a well plate consisting of aqueous volumes covered by carrier fluid (figure 3). The motorised linear stage, available from Standa, has a range of 100 mm with a 2.5 µm step and a load capacity of 6 kg in the vertical direction. A linear piece of capillary is connected to the stage and transverses in the vertical direction, figure 3, from carrier fluid to aqueous. This action, essentially a

micro-pipetting technique, permitted the creation of plugs of different volumes depending on the flow rate and the resident time in the aqueous phase. A CCD camera was used to determine the

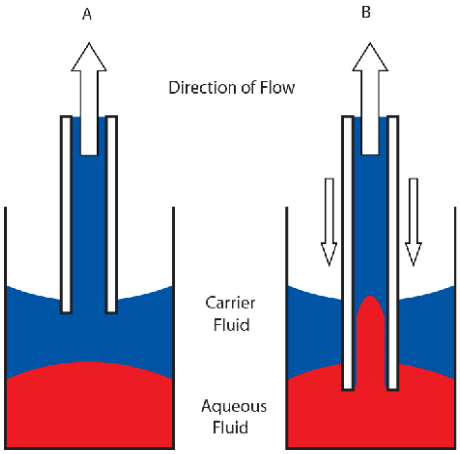


**Fig. 3** Illustration of droplet generation. Image A represents the system in single phase. Image B illustrates the capillary having traversed into the aqueous fluid. Plug length is proportional to flow rate and resident time in sample fluid.

plug length to within +/- 35 μm, by calculating the pixel to length ratio from an in-frame reference. The camera, a Sony DFW-SX900, uses a ½" CCD sensor chip. It has the ability of recording up to 7.5 frames per second at a resolution of 1280 x 960 colour pixels.

## 3. THEORY

Steady laminar flow in a capillary is governed by the Hagen-Poiseuille law:

$$Q = -\frac{\pi r^4}{8\mu}\left(\frac{dP}{dx}\right) \quad (1),$$

where $Q$ is the volumetric flow rate, $r$ is the radius of the capillary, $\mu$ is the absolute viscosity and $(dP/dx)$ the pressure gradient in the direction of flow. The Reynolds and Capillary numbers are:

$$\mathrm{Re} = \frac{\rho \overline{U} r}{\mu} \quad (2), \qquad Ca = \frac{\mu \overline{U}}{\sigma} \quad (3)$$

where $\overline{U}$ is the mean velocity, $\rho$ is the fluid density and $\sigma$ is the interfacial tension. The Hagen-Poiseuille law is analogous to Ohm's law for electrical circuits, where the pressure drop is analogous to the voltage, the volumetric flow rate to the current and the electrical resistance to the fluidic resistance:

$$R_{sp} = \frac{8\mu l}{\pi r^4} \quad (4)$$

This single phase fluidic resistance, $R_{sp}$, can then be defined as a constant by which the excess fluidic resistance, attributed to the second phase, can be measured against. The introduction of a second immiscible liquid changes the homogenous flow conditions into a segmented flow where the plug is convected along at a velocity that is dependant on the mean velocity and the thin film thickness. Accompanying this effect is an increase in the fluidic resistance over the single phase fluidic resistance despite the plugs having a significantly lower viscosity. A value for this increase in fluidic resistance due to the second immiscible phase is given by:

$$R' = \frac{R_P}{R_{sp}} \quad (5),$$

where

$$R_P = \frac{\delta P_P}{Q} \quad (6).$$

$R_P$ is the plug fluidic resistance, $\delta P_P$ is the measured liquid-liquid pressure drop and $Q$ is the flow rate. Pressure excess, $P_{ex}$, is defined here as the excess pressure over the single phase pressure, $P_{sp}$, due to the second immiscible phase:

$$P_{ex} = \delta P_P - P_{sp} \quad (7).$$

The Breatherton law (Aussillious and Quere, 2000) describes the relationship between the Capillary number and the film thickness:

$$\frac{h}{r} = 1.34 Ca^{2/3} \quad (8)$$

where $h$ is the film thickness. Kashid *et al.* (2007) modified a theoretical prediction by Charles (1963) by taking account of the water fraction to give:

$$\left(\frac{dP}{dx}\right)_h = \left(\frac{\alpha}{1-k^4}\right)\left(\frac{dP}{dx}\right)_{SP} \quad (9)$$

where $k = (r-h)/r$, and the subscripts h and SP stand for film thickness and single phase respectively. The equation relates the pressure drop along the thin film to the single phase pressure drop of the carrier fluid along the length of the capillary. The authors found a good agreement between the data (viscosity matched fluids) and the theoretical prediction, noting that the inclusion of internal circulation into the model would improve the accuracy of theoretical pressure drop predictions.

## 4. RESULTS

Three hydrodynamic effects are investigated, the capillary internal diameter, the effect of flow rate, and the effect the viscosity of the carrier fluid has on the pressure drop for immiscible aqueous plugs of a variety of volumes. All data sets employed PD5 as the carrier fluid unless otherwise stated. The introduction of a second immiscible fluid into the laminar flow regime significantly changes the hydrodynamic characteristics making it difficult to make an *a priori* design calculation. Figure 4 graphically illustrates the change in pressure signal over time with the introduction of four different plug lengths. The profile of the pressure signal (for bi-phasic flow) is independent of flow rate but dependant on the length of the aqueous plugs. After a sharp peak the signal decreases to a steady state value that is dependant on the length of the plug. The sharp peak was investigated using the same apparatus albeit with a high speed camera to monitor the aqueous plug in the liquid bridge junction.

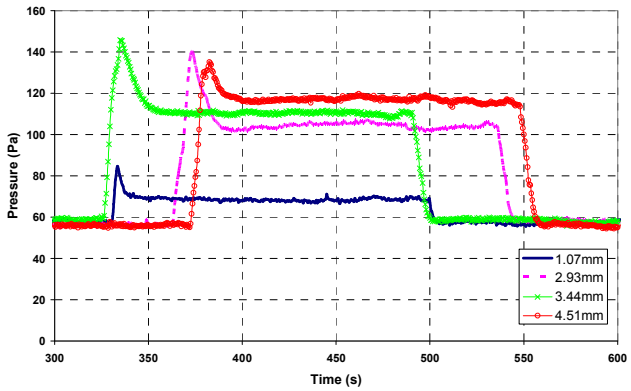


**Fig. 4.** Temporal pressure profile for four different aqueous plug lengths. $Q$ = 5 µl/min. $r$ = 200 µm. PD5 carrier fluid.

From the comparison of the real-time image acquisition with the pressure signal, it was determined that the pressure peak was due to a momentary blockage of the first liquid bridge. The pressure, at that point, remains constant while at the second liquid bridge, where the second pressure sense line is placed, reduces in pressure due to the constant flow rate. It is currently unclear why the magnitudes of the pressure peaks differ.

### 4.1. Capillary Diameter

In line with single phase laminar flow theory the internal diameter of a capillary has a significant effect in bi-phasic flow. Figure 5 illustrates the

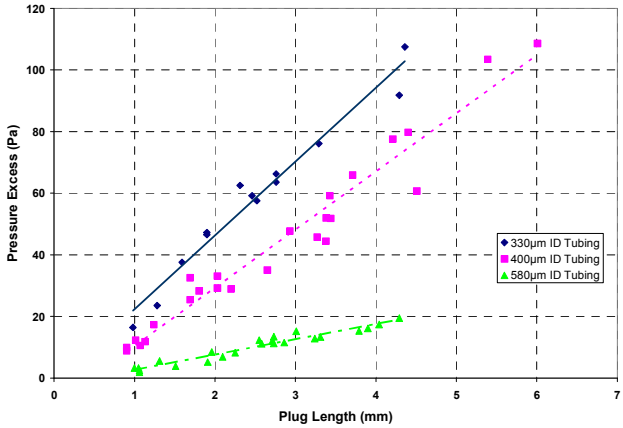


**Fig. 5.** Pressure difference for a range of plug lengths through three capillaries of different internal diameters. $Q$ = 5µl/min.

the difference in pressure excess for a range of plug lengths in three different capillaries at a constant flow rate. There is a clear linear trend between pressure excess and plug lengths for all capillaries. The divergence indicates a possible geometric relationship between the plug length and the capillary geometry.

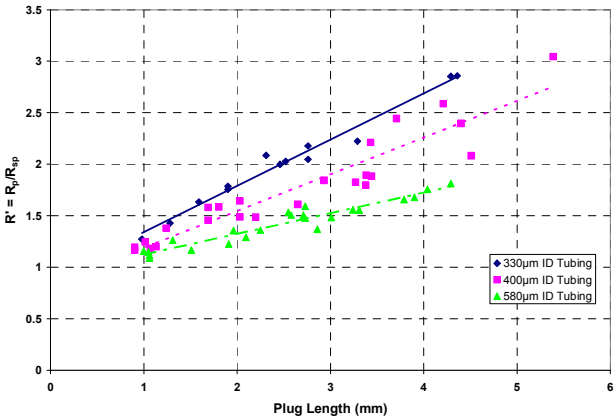


**Fig. 6.** Effect of capillary diameter on excess fluidic resistance for a range of plug lengths. $Q$ = 5µl/min.

Each data set is normalised against flow rate to give a value of excess fluidic resistance (figure 6). Where the trend lines cross the normalised resistance axis at one, a value for minimum plug length that causes no increase in fluidic resistance can be approximated. This value is the point where the fluidic resistance is same as the single phase fluidic resistance. This plug length approaches the capillary internal diameter giving a plug of spherical shape. The thin film, associated with the pressure and fluidic resistance excess, reduces to a point where it has a negligible effect.

A relationship between the plug length, the capillary diameter and the excess pressure was sought in order to develop a possible design correlation as this would be a useful tool for determining pumping requirements or flow distribution in complex microfluidic circuits used in µTAS. The data for each capillary was collapsed by making the pressure excess proportional to the plug length and inversely proportional to the square of the radius (figure 7). A possible reason for the divergence exhibited in the data to the right of the graph may be due to the development of internal circulations within the plug. King *et al.* (2006) noted the development of internal circulations from a low level to a high level at increasing plug lengths.

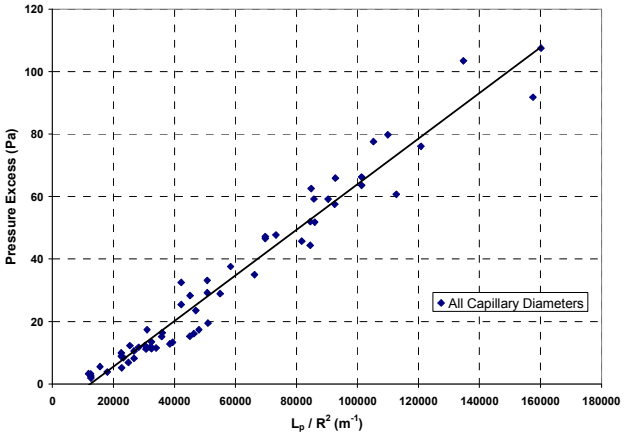


**Fig. 7.** Collapsed pressure data for three different capillary internal diameters through the geometric relationship. $Q$ = 5 µl/min. PD5 carrier fluid.

4.2. Flow Rate

Using a single capillary dimension, 400 µm internal diameter, the effect of flow rate on an immiscible liquid-liquid pressure drop was investigated. Figure 8 illustrates the effect for a range of plug lengths. As figure 8 illustrates, there is very little distinction between pressure excess at small plug lengths. As plug length increases, a greater divergence is exhibited between the data sets, indicating a more complex flow field developing in the plug. Figure 9, constructed from the same data sets, illustrates the flow rate effect on fluidic resistance. Counter intuitively there is a greater enhancement of fluidic resistance at a lower flow rate. The authors attribute this to the development of the thin film. Grimes *et al.* (2006) noted the development of the thin film with an increase in Capillary number. This hypothesis is also in accord with Charles's (1963) theory, who found that for laminar flow, the pressure gradient is a function of the diameter ratio.

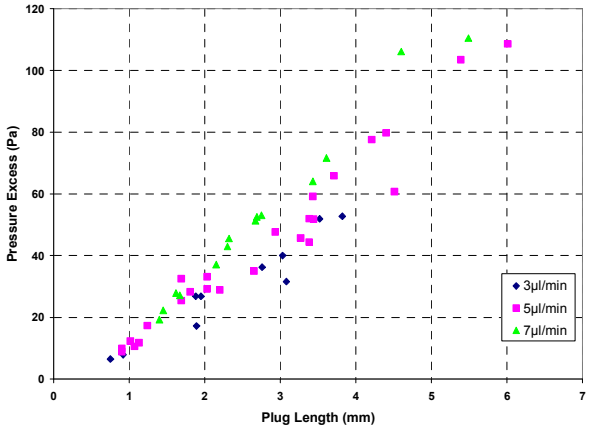


**Fig. 8.** Effect of flow rate on pressure excess in a bi-phasic system. Trend lines removed for clarity.

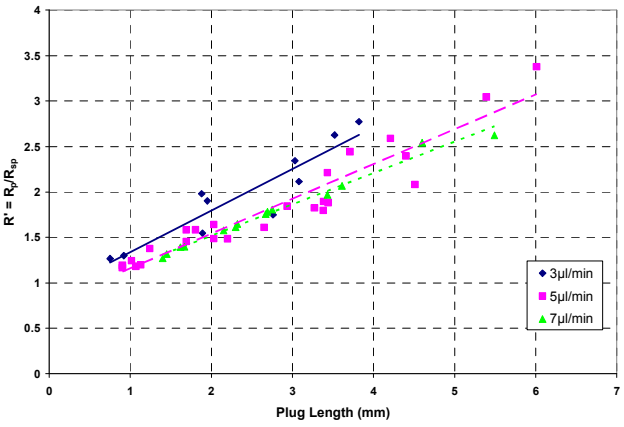


**Fig. 9.** Excess fluidic resistance versus plug length for three different flow rates. Minimum plug length for negligible fluidic resistance excess approximated at $R'$= 1. $r$ = 200 µm.

The lower flow rate also indicates a much lower tolerance for minimum plug length.

4.3 Theoretical Approximation

The Du Noüy ring method was used to determine the interfacial tension between the aqueous mix and the PD5 carrier fluid. Using this value, the

capillary number and hence the thin film thickness could be determined. The model proposed by Kashid *et al.* (2007) could then be applied to the experimental data. As figure 10 illustrates, the model, calculated from experimental parameters, shows a good comparison with the data for the 330 µm and 400 µm inner diameter capillaries. However the model over predicts the values for the 580 µm capillary. It is currently unclear as to why.

Similarly figure 11 illustrates the comparison between the model and the bi-phasic data for different flow rates. The model closely approximates the experimental data, however

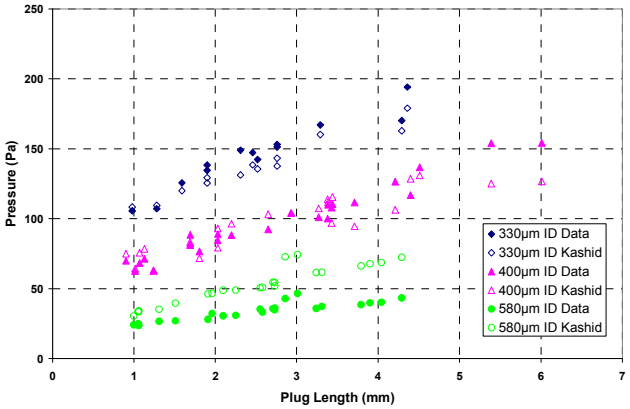


**Fig. 10.** Comparison of experimental data to theoretical model proposed by Kashid et al (2007) for all capillary. $Q$ = 5µl/min.

increasing flow rate and plug length increases the scatter in the values determined by the experimental model. This experimental data further validates of the model proposed by Kashid *et al.* (2007), for individual plug lengths and a different viscosity ratio.

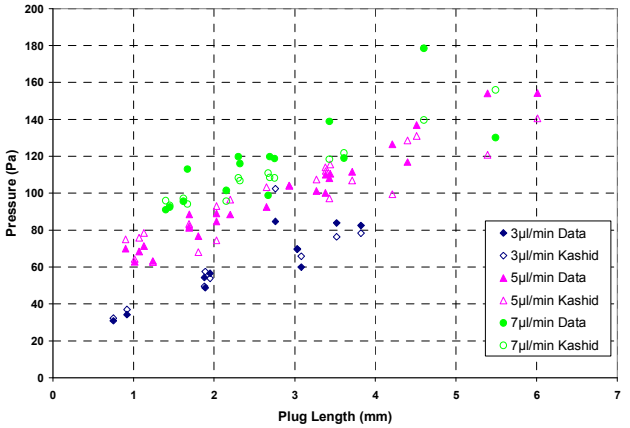


**Fig. 11.** Comparison of experimental data to theoretical model proposed by Kashid *et al.* (2007) for all flow rates. $r$ = 200 µm.

## 4.4 Carrier Fluid Viscosity

The effect carrier fluid viscosity has on the pressure drop across two different capillaries is investigated. As illustrated in figure 12 and 13, there is a clear difference between the pressure drop for a range of plugs lengths through the 400 µm and 580 µm capillaries. The large scatter evident throughout the 400 µm and towards the right of the 580 µm data sets is believed to be a result of and increase in the magnitude of the internal circulations through the momentum transfer across the plug carrier fluid interface (Malsche *et al.*, 2008). The higher viscosity fluid, AR20, exerts a larger shear on the fluid-fluid interface.

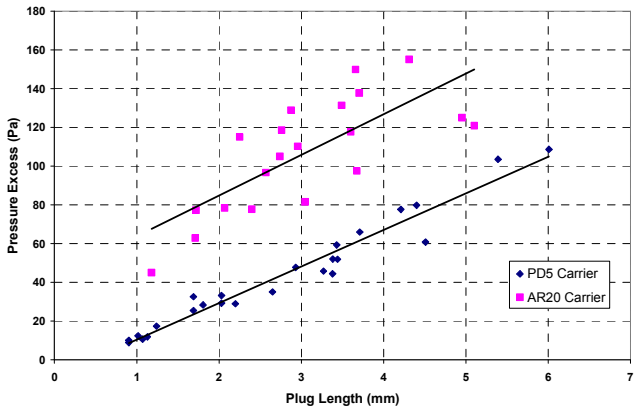


**Fig. 12.** Pressure increase versus plug length for two different carrier fluids in 400 µm internal diameter tubing. $Q$ = 5µl/min.

A clear linear trend is evident in the 580 µm data set with scatter developing at larger plug lengths, believed to be due to the onset of internal circulations within the plug.

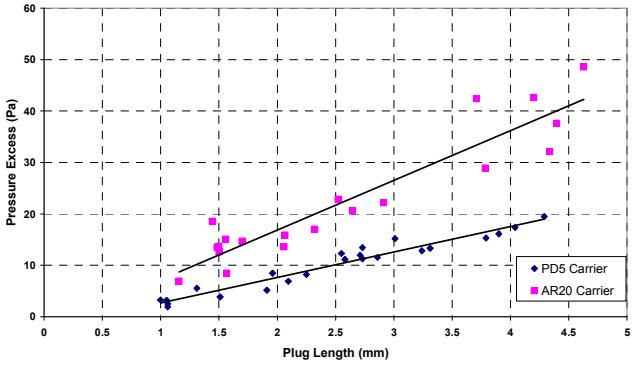


**Fig. 13.** Pressure increase versus plug length for two different carrier fluids in 580 µm internal diameter tubing. $Q$ = 5µl/min.

Figures 14 and 15 compare the fluidic resistance increase due to a second immiscible phase between two different carrier fluids. The viscous effects of the higher viscosity carrier fluid dominates over the effect the aqueous plug has on the fluidic resistance, highlighted by a lower *R*' for a given plug length.

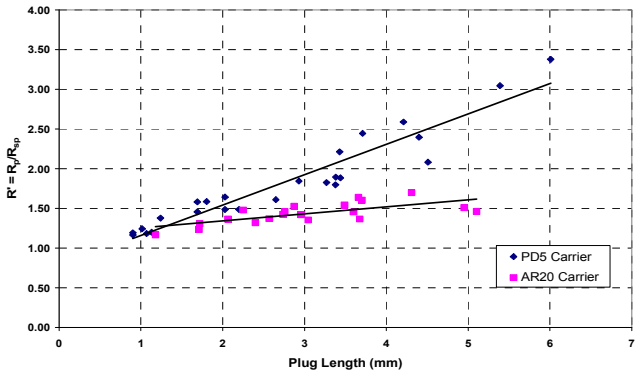


**Fig. 14.** Comparison between the fluidic resistance of two different carrier fluids for bi-phasic flow through 400µm internal diameter capillary. $Q$ = 5µl/min.

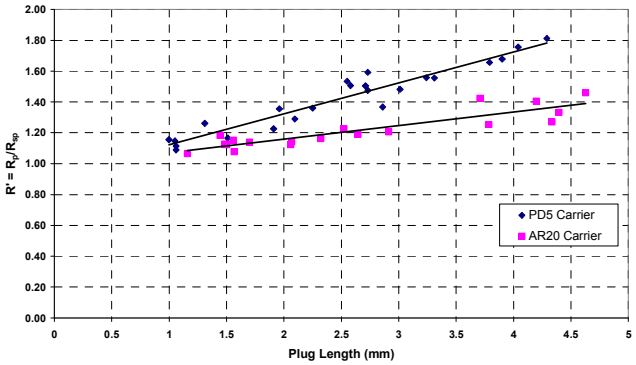


**Fig. 15.** Bi-phasic effect on fluidic resistance in 580 µm internal diameter capillary with two carrier fluids. $Q$ = 5µl/min.

## 4.5 Multiple Plug Trains

Using the 400 µm capillary the effect of two and three plug trains was characterised. Figure 16 illustrates the entrance and exit of three individual plugs through 100 mm of capillary. Entrance and exit of each plug is schematically represented in figure. Figure 17 compares each data set. Two and three plug trains also show a linear trend with an increase in total aqueous length. The spacing between the plugs ranges from 6-13 mm. This ensures redevelopment of the laminar parabolic velocity profile between the plugs. Malsch *et al.* (2008) found that the distance between aqueous plugs suspended in a carrier fluid had an effect on

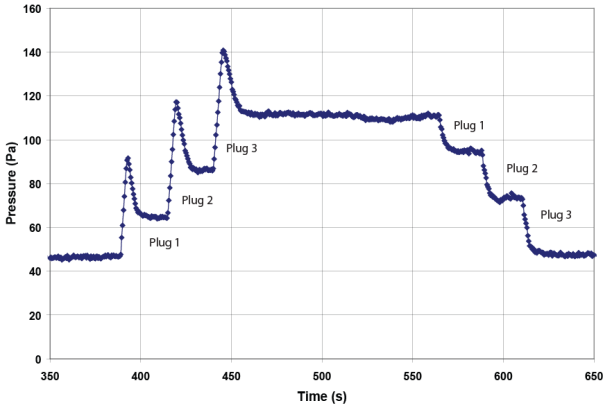


**Fig. 16.** Pressure-time profile for 3 plugs entering (left) and exiting (right) a capillary 100 mm in length. $Q$ = 5µl/min. $r$ = 200 µm.

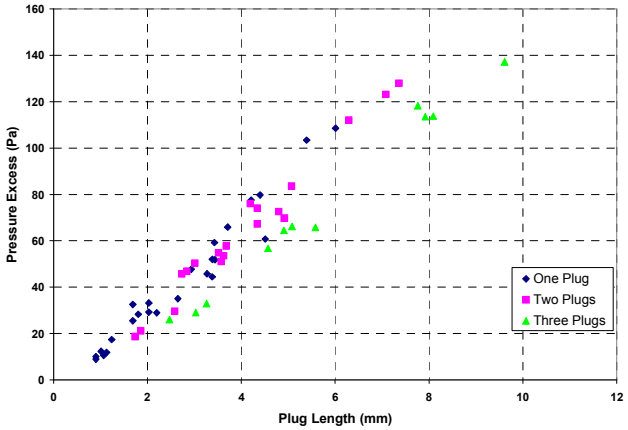


**Fig. 17.** Pressure excess versus plug lengths for single plugs, two and three plug trains (linear trend lines are absent for clarity). $Q$ = 5µl/min. $r$ = 200 µm.

the pressure drop. The authors suggested that this additional pressure would be based on the internal flow field of the carrier fluid between the plugs.

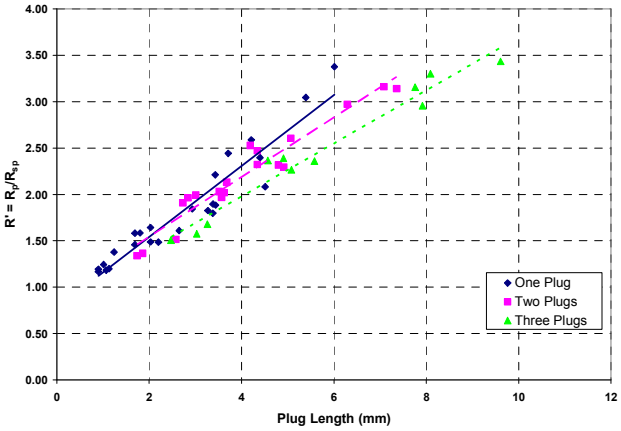


**Fig. 18.** Fluidic resistance versus plug lengths for single plugs, two and three plug trains. $Q$ = 5µl/min. data points indicative of total aqueous length. $r$ = 200 µm.

Evident in figures 17 and 18 is a reduced value for pressure excess and fluidic resistance with multiple aqueous plugs of similar length to a single plug length. It is believed that the low Reynolds flow causes a low contact angle hysteresis, reducing the effect the creation of more fluidic interfaces has on the liquid-liquid hydrodynamics.

## 5. Conclusions

The effect bi-phasic flow has on the pressure drop in a capillary was investigated under a number of different experimental conditions. It was shown that pressure excess increases linearly with plug length for a range of operational conditions. A theoretical model proposed by Kashid *et al.* (2007), based on the aqueous fraction and film thickness, exhibited good agreement with data. A useful design correlation was proposed based on the data from three capillaries. Analysis of data from two different carrier fluids highlights the need for a more thorough analysis of the complex flow fields in bi-phasic flow under different experimental conditions. A preliminary investigation of multiple plug hydrodynamics was carried out highlighting the need for a more comprehensive investigation.

## 6. Acknowledgements

The authors would like to thank Ryan Enright and the engineers at Stokes Bio for all their help and technical support.

## 7. References

- Adzima, B. J. and Velankar, S. S. 2006. Pressure Drops for Droplet Flows in Microfluidic Channels. J. Micromechanical and Microengineering 16, 1504-1510
- Aussillous, P. and Quéré, D. 2000. Quick Deposition of a Fluid on the Wall of a Tube. Physics of Fluids 12, 10 2367-2371
- Barrett, B., Davies, M. and Morris, A. 2007. Thermal Analysis of a Novel Continuous Flow Multi Layered PCR Device. Proc. ASME-JSME Thermal Engineering Summer Heat Transfer Conf. CD-ROM, #32792
- Burns, J. R., and Ramshaw, C. 2001. The Intensification of Rapid Reactions in Multiphase Systems using Slug Flow in Capillaries. Lab on a Chip 1, 10-15.
- Charles, M. E. 1963. The Pipeline Flow of Capsules: Part II Theoretical Analysis of Concentric Flow of Cylindrical Forms. Canadian J. of Chem. Eng. 46-50.
- Curran, K., Garvey, J., McGuire, D., Wyatt, P., Dalton, T. and Davies, M. 2007. A Continuous Flow Microfluidic Arrayer for Gene Expression Analysis. Qpcr, San Diego, available from http://www.healthtech.com/2007/qpc/index.ASP.
- Grimes, R., King, C. and Walsh, E. 2006. Film Thickness for Two Phase Flow in a Microchannel. ASME IMECE Conf. CD-ROM, #15882
- Groß, G. A., Thyagarajan, V., Kielpinski, M., Henkel, T. and Köhler, J. M. 2008. Viscosity-dependant Enhancement of Fluid Resistance in Water/Glycerol Micro Fluid Segments. Microfluidics and Nanofluidics 5, 281-287.
- Kashid, M. N., Gerkach, I., Goetz, S., Franzke, J., Acker, J. F., Platte, F., Agar, D. W. and Turek, S. 2005. Internal Circulation within the Liquid Slugs of a Liquid-Liquid Slug Flow Capillary Microreactor. Ind. Eng. Chem. Res 44, 5003-5010.
- Kashid, M. N. and Agar, D. W. 2007. Hydrodynamics of Liquid-Liquid Slug Flow Capillary Microreactor: Flow Regimes, Slug Size and Pressure Drop. J. Chem. Eng. 131, 1-13.
- King, C., Walsh, E. and Grimes, R. 2007. PIV Measurements of Flow within Plugs in a Microchannel. Microfluidics and Nanofluidics 3-4, 463-472.
- Malsch, D., Gleichmann, N., Kielpinski, M., Mayer, G. and Henkel, T. 2008. Effects of Fluid and Interface Interaction on Droplet Internal Flow in All-Glass Micro Channels. ASME-ICNMM, #62328.
- Miessner, U., Lindken, R. and Westerweel, J. 2008. Velocity Measurements in Microscopic Two-Phase Flows by means of Micro PIV. ASME-ICNMM, #62093.
- Roper, M. G., Easley, C. J. and Landers, J. P. 2005. Advances in PCR on Microfluidic Chips. Anal. Chem. 77, 3887-3894.
- Sarrazin, F., Loubière, K., Prat, L., Gourdon, C., Bonometti, T., and Magnaudet, J. 2006. Experimental and Numerical Study of Droplets Hydrodynamics in Microchannels. American Institute of Chemical Engineers. 52-12, 4061-4070.
- Sirr, N., Ciobanu, D., Grimes, R. and Davies, M. 2006. A Continuous Flow Polymerase Chain Reactor for DNA Expression Analysis. ASME-ACNMM, #96180.